Nanoscale

Incident Angle–Tuned, Broadband, Ultrahigh-Sensitivity Plasmonic Antennas Prepared From Nanoparticles on Imprinted Mirrors

Journal:	*Nanoscale*
Manuscript ID:	NR-ART-10-2014-005902.R1
Article Type:	Paper
Date Submitted by the Author:	13-Dec-2014

Complete List of Authors:	Yu, Chen-Chieh; National Taiwan University, Department of Materials Science and Engineering Tseng, Yi-Chuan; National Taiwan University, Department of Materials Science and Engineering Su, Pao-Yun; National Taiwan University, Department of Materials Science and Engineering Lin, Keng-Te; National Taiwan University, Department of Materials Science and Engineering Shao, Chang-Ching; National Taiwan University, Department of Materials Science and Engineering Chou, Sin-Yi; National Taiwan University, Department of Materials Science and Engineering Yen, Yu-Ting; National Taiwan University, Department of Materials Science and Engineering Chen, Hsuen-Li; National Taiwan University, Department of Materials Science and Engineering

Cite this: DOI: 10.1039/c0xx00000x

www.rsc.org/xxxxxx

PAPER

Incident Angle–Tuned, Broadband, Ultrahigh-Sensitivity Plasmonic Antennas Prepared from Nanoparticles on Imprinted Mirrors

Chen-Chieh Yu, Yi-Chuan Tseng, Pao-Yun Su, Keng-Te Lin, Chang-Ching Shao, Sin-Yi Chou, Yu-Ting Yen, Hsuen-Li Chen*

Received (in XXX, XXX) Xth XXXXXXXXX 20XX, Accepted Xth XXXXXXXXX 20XX
DOI: 10.1039/b000000x

We have used a low-cost, rapid, and direct imprint-in-metal method to prepare incident angle–tuned, broadband, ultrahigh-sensitivity plasmonic antennas from nanoparticles (NPs) and imprinted metal mirrors. By changing the angle of incidence, the nanoparticle-imprinted mirror antennas (NIMAs) exhibited broadband electromagnetic enhancement from the visible to the near-infrared (NIR) regime, making them suitable for use as surface-enhanced Raman scattering (SERS)–active substrates. Unlike other SERS-active substrates that feature various structures with different periods or morphologies, the NIMAs achieved broadband electromagnetic enhancement from single configurations. The enhancement of the electric field intensity in the NIMAs originated from coupling between the localized surface plasmon resonance of the NPs and the periodic structure–excited surface plasmon resonance (SPR) of the imprinted mirror. Moreover, the coupling wavelengths could be modulated because the SPR wavelength was readily tuned by changing the angle of the incident light. Herein, we demonstrate that such NIMAs are robust substrates for visible and NIR surface-enhanced resonance Raman scattering under multiple laser lines (532, 633, and 785 nm) of excitation. In addition, we have found that NIMAs are ultrasensitive SERS-active substrates that can detect analytes (e.g., rhodamine 6G) at concentrations as low as 10^{-15} M.

Introduction

Plasmonic antennas prepared from metallic nanoparticles (NPs) and metal mirrors have attracted great interest for their potential applications in surface-enhanced Raman spectroscopy (SERS),[1, 2] chemical and biological sensors,[3, 4] and atomic scale rulers.[5] The collective oscillation of free electrons in metallic NPs is influenced largely by their nearby environment. An NP can be regarded as a resonant dipole that will induce an image dipole on the underlying metallic mirror. Permittivity is a factor that defines the extent to which a material can be polarized; materials possessing higher permittivity are much more polarizable in the presence of external electrostatics. Therefore, the permittivity of the underlying substrate determines the strength of the induced image dipole.

Knight *et al.* demonstrated that the presence of a nearby dielectric substrate influences the frequency of the plasmon modes of metallic NPs.[6] When the permittivity of a dielectric substrate increases, the split in plasmon frequency becomes more obvious under both transverse electric (TE) and transverse magnetic (TM) polarization incidence. In addition, the dark-field scattering images and spectra of Au NPs immobilized on quartz, Si, and Au film are quite different: the dark-field scattering images of Au NPs immobilized on quartz substrates are solid whereas those for Au NPs immobilized on Si and Au films are donut-shaped.[2] These observations indicate that the scattering on high-permittivity substrates is dominated by dipoles oscillating in the vertical direction. Furthermore, NP–Au film systems exhibit the most obvious shifting of the plasmon wavelength under TM polarization incidence, suggesting strong interplay between the NPs and their image dipoles.[2, 7]

Typically, materials possessing high permittivity lead to more intense reflection of incident light. In visible and IR regimes, metals have high permittivity and high reflectance; as a result, their structures are applied widely in plasmonic antennas.[1-4, 8, 9] As mentioned above, a metal mirror will induce the most intense coupling between an NP and its image dipole, contributing to a dramatic enhancement in the strength of the electromagnetic field between them. The interaction between an NP and a metal mirror can also be explained in terms of plasmon hybridization of the localized plasmon in the NPs and the continuous surface plasmon supported by the metal mirror.[10] Therefore, metal mirrors are far more useful than other substrates in plamonic antennas—not only for their high permittivity but also because they support surface plasmon enhancement.

We suspected that imprinted metal mirrors possessing periodic structures would induce much stronger coupling to NPs as a result of periodic structure–excited surface plasmon resonance (SPR). Many studies have indicated that periodic metallic nanostructures—including nanohole arrays,[11-13] one-dimensional (1D) nanoslits,[14] and corrugated films[15, 16]—induce strong SPR in the visible and near-infrared (NIR) regimes and contribute to the extraordinary transmission (EOT).[11-16] Only a few such studies,

however, have concerned compound structures comprising metallic NPs and periodic structures. He *et al.* investigated the effect of localized surface plasmon resonance (LSPR) of metal NPs on EOT phenomena of nanohole arrays.[17] They found that changes in longitudinal and lateral displacement between the metal NPs and the nanohole arrays led to shifting and splitting of the EOT peak as a result of variations in the coupling strength and manner of the LSPR modes. In addition, the Wang group observed multiple SPR modes in a compound structure comprising NPs and nanohole arrays.[18] Moreover, Chen *et al.* revealed that the EOT of higher-order modes could be enhanced through the random embedding of Au NPs in periodic nanohole arrays.[19] Furthermore, Kofke *et al.* demonstrated that the size and orientation of the NPs and the period of nanoslit arrays all influenced the transmission wavelength, intensity, and bandwidth of composite NP/nanoslit arrays.[20] Notably, all previous studies have focused on the far-field EOT properties of the compound structures. To the best of our knowledge, there have been no investigations of the near-field electromagnetic enhancement induced by coupling between the LSPR of the NPs and the periodic structure-excited SPR.

SERS is a technique that enhances the Raman signals of analytes; such signals provide information about the chemical bonding and symmetry of a molecule because every molecule has its own specific Raman fingerprint. The mechanism of SERS is dependent on two effects: chemical enhancement and electromagnetic enhancement.[21] Chemical enhancement is based on charge transfer between the analyte and the SERS-active substrate; it can enhance the Raman signals by one or two orders of magnitude. Electromagnetic enhancement is a more dominant effect when the analyte is adsorbed on plasmonic nanostructures. The strong local electric field around the plasmonic nanostructures leads to a dramatic enhancement in the intensity of the Raman signals of the analyte. Accordingly, SERS-active substrates possessing large electric field intensities are preferred, as are those exhibiting broadband plasmonic enhancement. Multiple excitation laser lines can be employed in SERS measurements. For example, resonance Raman spectroscopy typically uses laser lines in the visible regime, because most dye materials absorb visible light.[22-24] NIR laser lines can be used to suppress the background fluorescence of analytes that can occur when illuminating with visible light.[25] UV laser lines are commonly applied to excite the Raman signals of biomolecules (e.g., proteins, DNA) and suppress their background fluorescence.[26, 27] Therefore, the laser line is often chosen judiciously according to the analyte in question. Accordingly, a SERS-active substrate exhibiting broadband plasmonic enhancement would be more suitable for applications requiring excitation from multiple laser lines than would one responding to only a single resonance wavelength. Pasquale *et al.* demonstrated that broadband plasmonic enhancement in metal NP necklaces occurred as a result of a strong photonic–plasmonic coupling effect;[28, 29] the diameter and number of particles in the necklace had great influence on the plasmonic properties, with the necklace's structure being optimized when the particle diameter was an integer multiple of the wavelength. In addition, the Aouani and Navarro-Cia group has reported multiresonant broadband optical antennas having a trapezoidal configuration, with the broadband properties arising from overlapping of various dipole resonances excited across the nanoantenna;[30-32] the operation of these antennas was, however, focused on the electric field enhancement in the IR regime, making them not suitable for SERS. Multiresonant antennas can be achieved by embedding conventional dimer gap or bow-tie nanoantennas into multiple-periodic gratings allowing broadband plasmonic enhancement in the visible and NIR regimes.[33] A serious drawback of this configuration is, however, that the positions of the electromagnetic hot spots would change in response to the resonance wavelength, thereby limiting its applications on SERS-active substrates. Moreover, although these optical antennas are claimed to exhibit broadband enhancement, comparisons of SERS measurements performed with excitation from different laser lines have not been reported. Furthermore, these broadband antennas have all been designed with complicated configurations.

Focused ion beam (FIB) and electron beam lithographies are generally adopted when fabricating metallic substrates possessing periodic structures with well-defined diameters and spacings. These methods are, however, very expensive and provide low throughput. On the other hand, nanoimprint lithography has the attractive properties of allowing high-throughput, rapid fabrication of structures over large areas;[34-36] as a result, it can be used to fabricate a variety of metallic nanostructures. Many groups have employed nanoimprint lithography to shape photoresists or polymers; subsequent reactive ion etching (RIE), deposition of metal films, and lift-off processes can then be used to obtain the metallic nanostructures. Because of plasmon resonance, such metallic nanostructures might act as SERS-active substrates. For example, Li *et al*. used nanoimprint lithography to fabricate SiO_2 pillars, with deposition of metal films and self-assembly of NPs leading to unique disk-coupled dots-on-pillar antenna array (D2PA) plasmonic structures;[37] these three-dimensional (3D) antenna arrays provided large electromagnetic enhancement as a result of coupling between the nanodots and the 3D cavities. Alvarez-Puebla *et al.* used nanoimprint lithography to pattern and fabricate silicon gratings and pillars of various diameters; subsequent deposition of Ag island films covering the gratings or pillars resulted in SERS-active substrates.[38] Because of differences in the morphologies and diameters of these plasmonic gratings or pillars, the plasmon wavelength could be shifted for a particular SERS application. Broadband properties could be achieved, however, only when preparing various plasmonic structures with different morphologies and diameters; that is, a single structure could not be used for different laser lines.

In this study, we applied a one-step direct nanoimprint-in-metal method to rapidly fabricate periodic structures on Ag mirrors. Without requiring a photoresist, RIE, or lift-off processing of conventional nanoimprint lithography, we could obtain large-area imprinted mirrors with well-defined periods and morphologies in a single step. We fabricated broadband plasmonic antennas featuring a simple configuration: metal NPs on an imprinted mirror. The broadband plasmonic enhancement of the NP-imprinted mirror antennas (NIMAs) originated from coupling between the LSPR of the NPs and the periodic metallic structure–exited SPR. The resonance wavelength of a periodic structure–excited SPR depends on the metal material, the

environmental dielectric, the period of the nanostructure, and the angle of the incident light. Therefore, its SPR wavelength is broadband-tunable by controlling the excitation conditions. Typically, the gap spacing and the refractive index of the dielectric spacing will determine the plasmon wavelength of an NP–mirror antenna (NMA).[1, 5, 9] Here, we found that the plasmonic coupling wavelength of a NIMA with a fixed gap spacing and dielectric spacer could be finely tuned only by varying the oblique incidence, due to shifting of the periodic structure–excited SPR. This observation implies that a single NP-imprinted mirror structure can be used as a broadband-tunable antenna suitable for surface-enhanced resonance Raman spectroscopy (SERRS) with high sensitivity.

Results and discussion

Fig. 1 provides a schematic illustration of the fabrication processes of the imprinted Ag mirror and a NIMA. We employed nanoimprint in metal lithography to texture the Ag mirrors. Using electron beam lithography, we fabricated a Si mold having 1D gratings with a period of 400 nm. We then used DC sputtering at a rate of 3 Å/s to deposit 50-nm-thick Ag mirrors on polycarbonate (PC) substrates. Next, we imprinted Si molds on the Ag mirrors under various pressures at 150 °C (the glass transition temperature of PC). After the first imprinting step, we rotated the Si mold by 90° (i.e., perpendicular to the first grating) and imprinted the textured mirror again. Using this two-time nanoimprint-in-metal method, we fabricated two-dimensional (2D) periodic nanostructures on the Ag mirrors. The period of the Si mold defined the period of the grating structures on the textured Ag mirror; the imprint pressure influence the depth of the structures. We obtained NIMAs by self-assembling Ag NPs onto the imprinted Ag mirrors (Fig. 1b and 1c). The NPs are randomly distributed on the imprinted Ag mirror. Some 2D nanoclusters were observed on the imprinted Ag mirror, and these nanoclusters would increase the number of hot spots that enhanced the Raman signals. Notably, in NIMA and NMA system, the main electromagnetic enhancement came from the out-of-plane coupling between the NPs and the underlying mirror, but the 2D nanoclusters would demonstrate both in-plane and out-of-plane plasmonic coupling. Therefore, the SERS performance of the NIMA or NMA would not be reduced when some nanoclusters are present. The overall average density of NPs by our self-assembling process was ca. 6 particles/μm^2. And the 3D configuration of a NIMA could be observed from the tilted SEM images in the lower inset of Fig. 1c.By changing the angle of incidence, the NIMAs were potential broadband SERS-active substrates for various laser line excitation lines (see Fig. 1b and following discussion).

We compared the morphologies of the imprinted mirrors prepared using different imprinting pressures. The imprinted mirror featured an irregular, rough surface when the imprinting pressure was relatively low (ca. 1 MPa; Fig. 2a). This low imprint pressure induced plastic deformation of the metal surface, but the extent of deformation was not sufficiently large to replicate the morphology of the Si mold, resulting in the irregular, roughen surface. When we increased the imprinting pressure, the metal surface displayed the periodic structure copied from the mold and the structures became deeper (Fig. 2b and 2c). For the imprinted mirror prepared at 3 MPa, the depth of the structure was

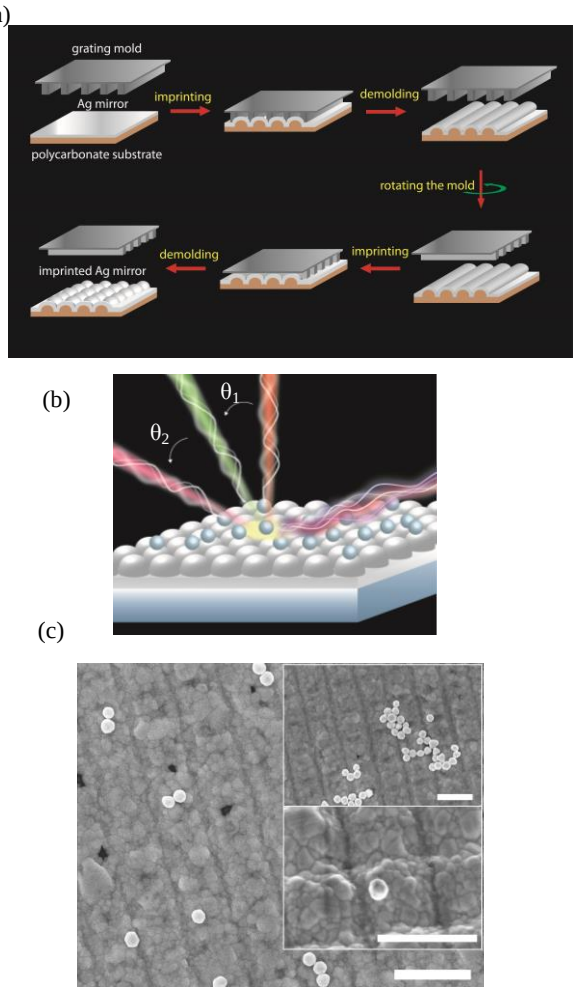

Fig. 1 (a, b) Schematic representations of (a) the fabrication of an imprinted Ag mirror using a two-step imprint-in-metal method and (b) a NIMA; by changing the angles of incidence, the NIMA behaved as a broadband SERS-active substrate for excitation using different laser lines. (c) SEM image of a NIMA; some isolated Ag NPs and Ag nanoclusters are decorated on the imprinted Ag mirror. Inset: tilted SEM image of an isolated Ag NP on the imprinted Ag mirror. The scale bars are 500nm.

approximately 70 nm; when we increased the imprinting pressure to 5 MPa, the structure depth increased to approximately 100 nm and the structure had much steeper sidewalls. Although a higher imprinting pressure increased the structure depth, more importantly it also provided more-accurate mold-copied structures. Notably, we found that a 100-nm-deep structure could excite the SPR efficiently.

Our imprinted mirrors with 2D periodic structures exhibited SPR phenomena in the visible and NIR regimes. We investigated the SPR modes of the imprinted mirror under an imprinting pressure of 5 MPa. We collected zero-order transmission spectra of the imprinted mirror, measured with incident angles ranging from 0 to 65° at an increment of 5°, to form the SPR dispersion diagram. The corresponding angle-dependent zero-order transmission spectra were provided in supplementary information (Fig. S1). Fig. 3 displays the measured SPR dispersion diagram, and the yellow dash lines indicated the shifting and splitting of

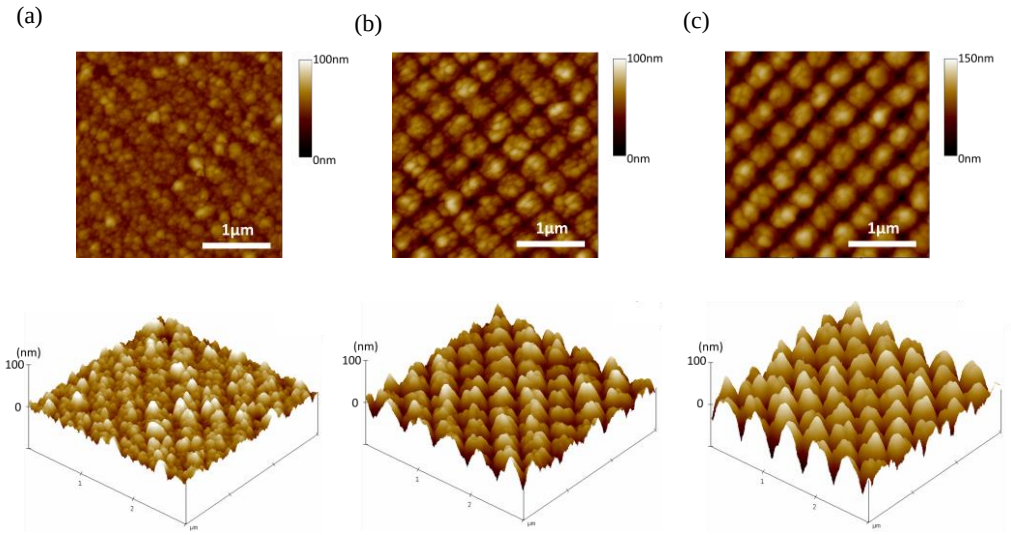

Fig. 2 Top-view and 3D AFM images of imprinted Ag mirrors (period: 400 nm) prepared using imprinting pressures of (a) 1, (b) 3, and (c) 5 MPa.

SP modes. Generally, the wavevector of surface plasmon (k_{SP}) can be expressed as:[39]

$$k_{SP} = k_x \pm nG_x \pm mG_y \quad (1)$$

where the $k_x = (2\pi/\lambda)\sin\theta$ is the component of the incident photon's wavevector in the plane of the grating, and $G_x = G_y = (2\pi/a_0)$ are the grating momentum wavevectors for a square array. The *n*, *m* are the order numbers of the grating momentum wavevectors, and (*n*, *m*) are generally assigned as the SP mode indices. Therefore, if the incident angle (θ) is varied, the incident light excites different SP modes. The SP modes [(1, 0), (1, 1), (2, 0), etc.] would split into positive and negative modes under oblique incidence. Accordingly, we plotted the yellow dash lines on the dispersion diagram to indicate the shifting and splitting of the corresponding SP modes. When under normal incidence, the (1, 0) mode was excited at a wavelength of 630 nm, whereas the (1, 1) mode was induced at a wavelength of 450 nm. The imprinted mirror had the attractive feature of a broadband-tunable SPR mode under oblique incidence. The –(1, 0) mode shifted from 630 to 950 nm, whereas the +(1, 0) mode shifted from 630 to 450 nm, when we changed the angle of incidence from 0 to 60°. On the other hand, the –(1, 1) mode covered the wavelength regime from 450 to 750 nm and the +(1, 1) mode was located in the wavelength regime of less than 450 nm. For SERS applications, the SPR wavelength should coincide with the wavelength of the excitation laser. For SERS measurements through laser excitation at 532 nm, the SPR could be induced at an angle of incidence of 15° [–(1, 1) mode] or 25° [+(1, 0) mode]. Besides, to match the laser excitation at 633 nm, the SPR could be excited at 0° [(1, 0) mode] or 35° [–(1, 1) mode]. Moreover, for laser excitation at 785 nm, the angle of incidence could be approximately 23° [–(1, 0) mode]. Therefore, the imprinted mirror could be utilized in SERS measurements under various laser lines of excitation.

Previously, NMAs have been used in SERS measurements under oblique incidence. Mubeen *et al*. proved that the SERS efficiency was enhanced upon increasing the angle of incidence.[1] They changed the plasmon wavelength of the antenna by using gap spacers with different refractive indices; nevertheless, the wavelength regime was confined between only 550 and 700 nm. Typically, the plasmon wavelength of an NMA is determined by the refractive index and the thickness of the spacer. It is very difficult to achieve a broadband working antenna using just a single NMA structure. Antennas with different gap spacers or dielectrics must be employed to match the excitation laser wavelength. Therefore, our NIMA was superior to the NMA in terms of its additional SPR enhancement and broadband tunability. We could use a single NIMA (i.e., refractive index and thickness of the spacer both fixed) to achieve a broadband SERS-active substrate by simply changing the angle of incidence. Moreover, the electromagnetic enhancement of the NIMA covered wavelengths from the visible to the NIR regime (Fig. 3).

Next, we compared the SERS performances of the NMA and NIMA using different laser lines for excitation. First, we tested the two distinct antennas under laser excitation at 532 nm to compare their SERS performances. Fig. 4a and 4b display the measured SERS spectra of 10^{-6} M rhodamine 6G (R6G) on both the NMA and NIMA excited under TM-polarized light at a wavelength of 532 nm at angles of incidence of 15 and 25°, respectively. On the imprinted mirror, these two angles of incidence, 15 and 25°, corresponded to the excitation conditions of the –(1, 1) and +(1, 0) SPR modes, respectively, at 532 nm. Therefore, we expected that the coupling between the LSPR of the NPs and the SPR on the imprinted mirror would greatly enhance the SERS performance. In addition to dipole and image dipole coupling, as in the case of the NMA, the imprinted mirror

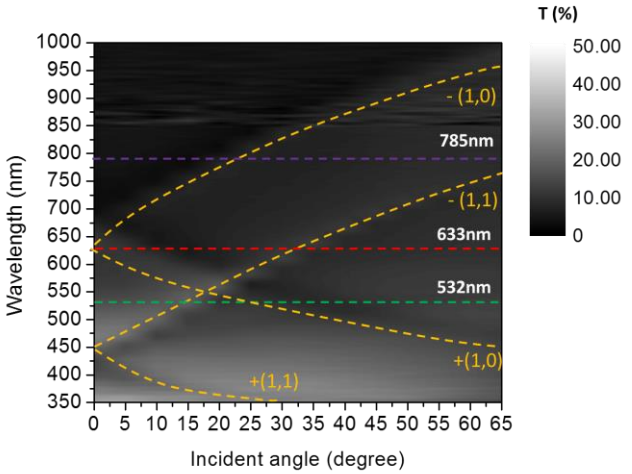

Fig. 3 SPR dispersion diagram of an imprinted Ag mirror having a period of 400 nm. The dispersion diagram was the collection of zero-order transmission spectra of the imprinted mirror, measured with incident angles ranging from 0 to 65° at an increment of 5°.

also introduced SPR enhancement; thus, the electric field intensity was larger in the NIMA than that in the NMA. As revealed in Fig. 4a and 4b, the intensity of the signals in the SERS spectra of R6G adsorbed on the NIMA were higher than those on the NMA.

Next, we tested the SERS measurements with laser excitation at 633 nm. Based on the SPR dispersion diagram in Fig. 3, a single imprinted mirror would induce the (1, 0) SPR mode at 0° and the –(1, 1) SPR mode at 35° incidence under excitation at 633 nm. Therefore, if we wished to obtain SERS spectra of R6G under excitation at 633 nm, we could simply change the angle of incidence to 0 or 35°. Fig. 4c and 4d compare the SERS spectra of R6G adsorbed on the NMA and NIMA under excitation at 633 nm with angles of incidence of 0 and 35°, respectively; clearly, the SERS performance of the NIMA was better than that of the NMA under these conditions. Because the excitation wavelength (633 nm) was far from the plasmon wavelength of the NMA, the electric field intensity on the NMA decreased, as did the SERS performance. On the other hand, because of the periodic structure–excited SPR, electromagnetic coupling between the NPs and the imprinted-mirror remained intense; therefore, the NIMA functioned well under excitation at 633 nm. The working spectral range of the NIMA was not only in the visible regime but also in the NIR regime. By changing the angle of incidence to 25°, the –(1, 0) SPR mode of the imprinted mirror was excited at 785 nm. As displayed in Fig. 4e, the signals in the SERS spectrum of R6G had high intensity when using the NIMA as the SERS-active substrate. Therefore, the NIMA is a broadband-tunable SERS-active substrate that possesses high electric field intensity over the visible and NIR regime.

To verify the influence of the periodic structure–excited SPR, we measured the SERS spectra of R6G adsorbed on the NIMA and NMA under different excitation wavelengths at an angle of incidence of 50°. We chose this angle based on the SPR dispersion diagram in Fig. 3; the periodic structure–excited SPR in this study would not be induced at 50° for any laser source (532, 633, or 785 nm). Fig. 4f–h display the SERS spectra of R6G adsorbed on the NIMA and NMA under different excitation wavelengths at 50°. When the angle of incidence mismatched the excitation conditions for SPR, the coupling between the NPs and the imprinted mirror was similar to that in the NMA. Therefore, the SERS signals obtained from the NIMA were only very slightly greater than those of the NMA (Fig. 4f–h). These findings confirmed that the periodic structure–excited SPR played an important role in the electromagnetic enhancement in the NIMA. When the angle of incidence was mismatched, the SPR could not be induced at any of the laser wavelengths, leading to lower degrees of enhancement of the SERS signals. Nonetheless, even under mismatched conditions, the NIMA exhibited SERS performance that was comparable to or slightly greater than that of the NMA. We provided the angle-dependent SERS intensity ratio (I_{NIMA}/I_{NMA}) of 1360 cm^{-1} R6G fingerprints in Fig.S2. The excitation wavelength was 532nm. Here we did not provide the angle-dependent SERS spectra due to the following reasons. First of all, in addition to the SPR enhancement, the intensity of the electric field normal to the NMA or NIMA surface (E_Z) would increase upon increasing the angle of incidence due to the different LSPR coupling strengths. Second, the input excitation power density on the sample surface would decrease under large incident angles due to the broadened illumination area. The two reasons mentioned above would both influence the SERS intensity of NIMA and NMA. Therefore, we proposed the SERS intensity ratio between NIMA and NMA under the same incident angles would be much more proper to indicate the SPR effect. The ratio of 1360 cm^{-1} R6G fingerprint revealed an obvious enhancement in the resonance angles, which clearly showed that the plasmonic coupling between Ag NPs and the underlying imprinted Ag mirrors greatly enhanced the SERS performance.

The outstanding SERS performance of the NIMA originated from the great electromagnetic enhancement provided by coupling between the LSPR of the NPs and the SPR of the imprinted mirror. Here, we used the three-dimensional finite difference time domain (3D-FDTD) method to simulate the electric field intensities in both the NMAs and NIMAs. Fig. 5a displays the simulation model that we employed in this study. We assumed a random distribution of the NPs on both the textured mirror and the flat mirror. The simulation volume (a unit cell) was 1200×1200×800 nm^3. The grid sizes were 8 nm in the x, y direction and 1nm in the z direction. The unit cell was repeated periodically in the x and y direction, and perfect matched layer (PML) was adopted in the boundary of z direction. A TM-polarized plane wave was assumed in the simulation. The incident angles were dependent on the incident wavelengths [based on the SPR dispersion diagram (Fig. 3)]—15° and 25° for 532nm, 0° and 35° for 633nm, and 25° for 785nm. We calculated the Raman signal enhancement ($|E_z/E_0|^4$) on the antenna surface in the simulation domain (enclosed by the dashed red line). Fig. 5b provides the averaged Raman signal enhancement. The Raman signal enhancements of the NIMA were stronger than those of the NMA under excitation wavelengths of 532, 633, and 785 nm at the proposed angles of incidence. The strongest Raman signal enhancement (ca. 6×10^6) for the NIMA occurred when the frequencies of the LSPR of the NP dimer (the NP and its

Cite this: DOI: 10.1039/c0xx00000x

www.rsc.org/xxxxxx

PAPER

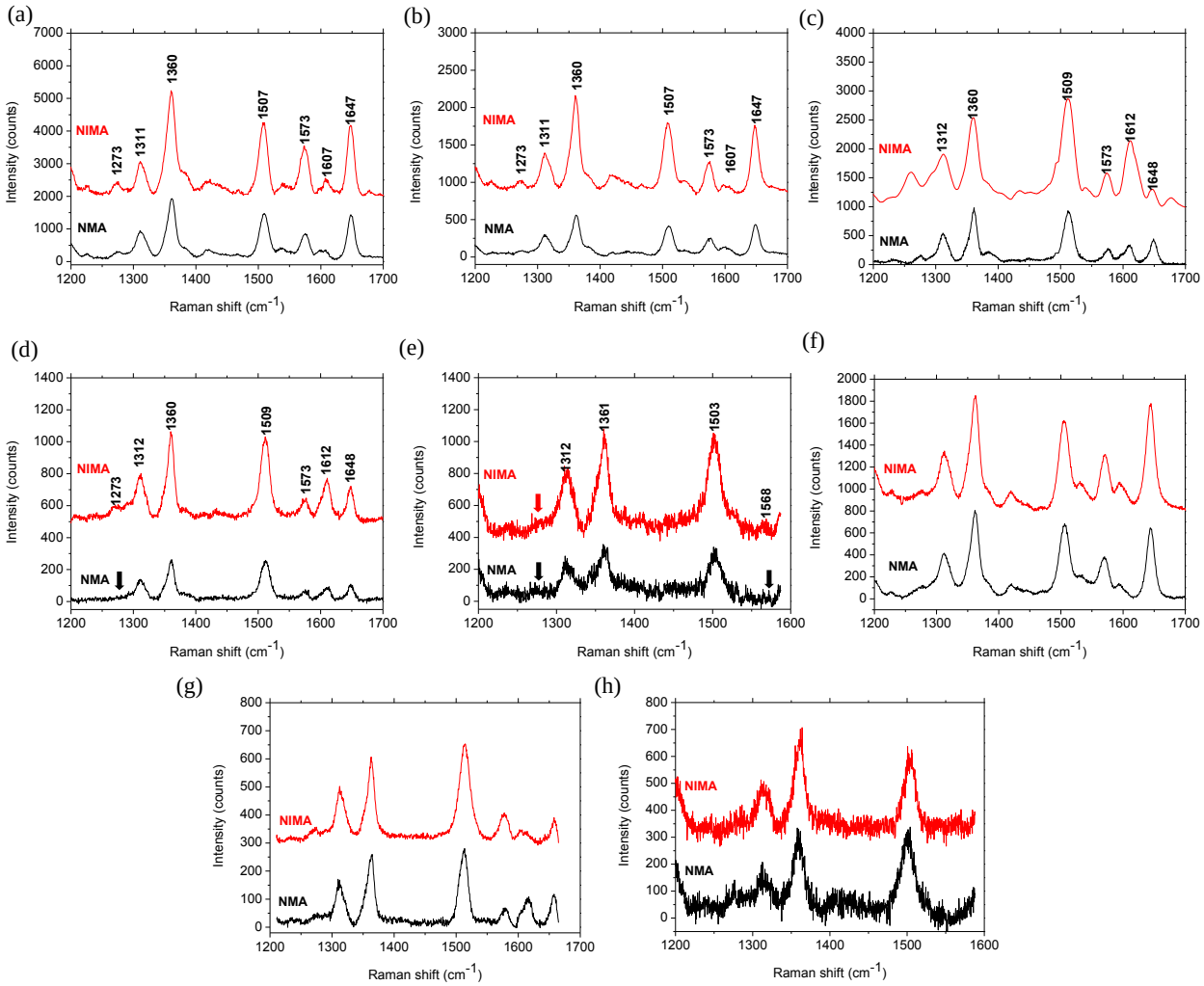

Fig. 4 SERS spectra of 10–6 M R6G adsorbed on NP-mirror and NP-imprinted mirror antennas under excitation at (a, b, f) 532 nm with angles of incidence of (a) 15, (b) 25, and (f) 50°; (c, d, g) 633 nm with angles of incidence of (c) 0, (d) 35, and (g) 50°; and (e, h) 785 nm with angles of incidence of (e) 25 and (h) 50°. The arrows in (d) and (e) indicate the missing Raman lines of R6G.

image dipole) and the periodic structure–excited SPR of the imprinted mirror were coincident (ca. 532 nm). Electromagnetic coupling between the two surface plasmons resulted in great enhancement of the electric field intensity and, thus, the Raman signal enhancement. Although wavelengths of 633 and 785 nm were far from the LSPR regime of the NP dimer, the periodic structure–excited SPR still featured intense electromagnetic coupling between the NPs and the imprinted mirror. The Raman signal enhancement was more obvious at larger angles of incidence. Because electromagnetic coupling was induced in a direction normal to the mirror surface, the electric field oscillating in this direction dominated the Raman signal enhancement. Under oblique incidence, the incident TM-polarized light would contribute more to the electric field component normal to the mirror surface; therefore, plasmonic coupling became more apparent and led to a greater enhancement of the Raman signals. For example, the Raman signal enhancement was greater at 25° than at 15° under excitation at 532 nm; in addition, the enhancement was greater at 35° than at 0° under excitation at 633 nm. Notably, in the NMA system, there was negligible coupling between the NPs and the underlying flat mirror at normal incidence with excitation of 633 nm because there was no normal component of the incoming electric field. On the other hand, in the NIMA system, the imprinted mirror would induce a surface plasmon polariton propagating along the surface and possessing an electric field oscillating in the direction normal to the surface. Therefore, plasmonic coupling was possible even when the system was under excitation at normal incidence; this

feature was absent in the NMA system.

We have demonstrated that the SERS performance of our NIMA was much better than that of the previously reported NMA. This improved performance originated from plasmonic coupling between the NPs and the underlying imprinted mirror. The periodic metal structures on the imprinted mirror excited the SPR.

The structural depth would have a large influence on the coupling efficiency of the incoming light into surface plasmon polariton;

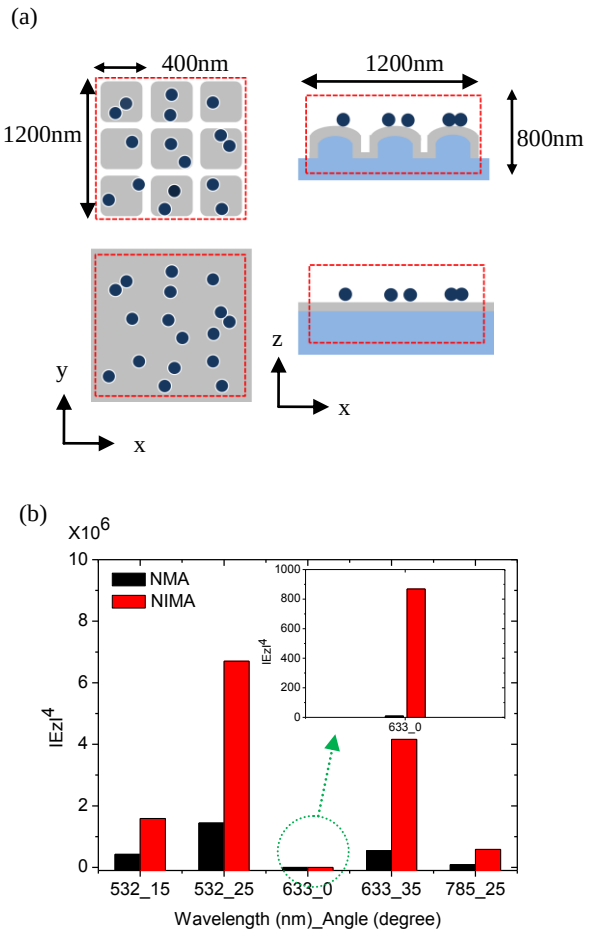

Fig. 5 (a) Schematic 3D-FDTD simulation models of the NMA and NIMA. The dashed red line encloses the simulation domain: a 1200 nm × 1200 nm × 800 nm unit cell that periodically repeated in x-y plane. (b) Average electric field enhancement in the NMA and NIMA.

therefore, it would influence the Raman signal enhancement. Fig. 6 compares the SERS performances (excitation at 633 nm; 0 and 35° incidence) of the NIMAs prepared under imprinting pressures of 1, 3, and 5 MPa; Fig. 2 presents the corresponding morphologies. When we increased the imprinting pressure, the consistency of the textured structures and the deeper trenches resulted in significant coupling of the incoming light into the surface plasmon polariton, leading to more intense SPR. The SERS spectra reveal that the intensity of the Raman signals increased when using the NIMAs prepared at higher imprinting pressures. This observation implies that the SPR from the imprinted mirror did indeed contribute to the SERS enhancement, as proposed.

In addition to the trench depth, the plasmonic modes also influenced the coupling efficiency and strength between the NPs and the imprinted mirror. Typically, the resonance intensities of lower-order plasmonic modes are greater than those of higher-order ones. Therefore, using a lower plasmonic mode to the working wavelength regime is preferred. Here, we prepared two different NIMAs having periods of 400 and 800 nm, respectively.

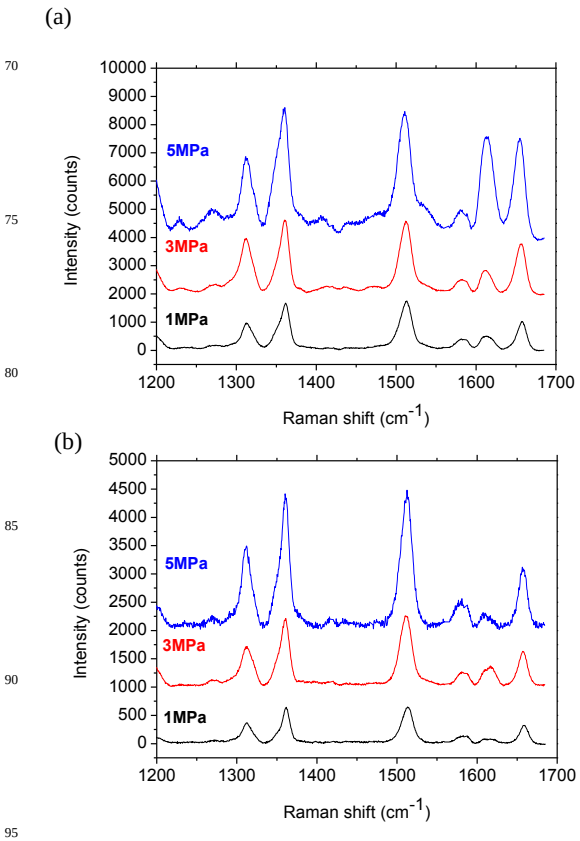

Fig. 6 SERS spectra of 10^{-6} M R6G adsorbed on NIMAs prepared using various imprinting pressures, under excitation at 633 nm with angles of incidence of (a) 0 and (b) 35°.

Fig. 7a displays top-view and 3D AFM images of the imprinted Ag mirror having a period of 800 nm. Fig. 3 and 7b present SPR dispersion diagrams of the NIMAs having periods of 400 and 800 nm, respectively. As the SPR dispersion diagram indicates, the fundamental SPR mode of the NIMA having a period of 800 nm was excited in the NIR regime, whereas that of the NIMA having a period of 400 nm was induced in the visible regime. We obtained SERS measurements under excitation at 633 nm at an angle of incidence of 35°, where the –(1, 1) and –(2, 0) modes for the NIMAs were located for the structures having periods of 400 and 800 nm, respectively. Fig. 7c presents SERS spectra of 1 μM R6G adsorbed on the two NIMAs. The NIMA having a period of 400 nm enhanced the intensity of the Raman signals to a greater extent than did the NIMA having a period of 800 nm. As described above, the electric field enhancement of the NIMA came from electromagnetic coupling between the LSPR of the NPs and the SPR of the underlying imprinted mirror; therefore, the intense SPR would contribute to stronger coupling. By

changing the period of the metallic structures on the imprinted mirror as well as the angle of incidence, we could obtain broadband antennas for SERS and SERRS.

SERRS is a technique that enhances the Raman signals of analytes adsorbed on metallic nanostructures by matching the excitation laser wavelength to both the absorbance regime of the analytes and the plasmon wavelength of the metallic nanostructures.[22-24, 26, 27] Matching the excitation laser wavelength to the absorption band of the analytes can contribute additional resonance enhancement to the SERS. Previously, NP-based SERS substrates have been synthesized with NPs featuring various complicated morphologies, including nanorods,[40] nanostars,[41] nanobranches,[42] and nanoshells,[43] for operation at different working wavelengths. These NPs did not, however, function over a broadband working regime because their LSPRs could be excited at only specific wavelengths. In the NMA or other SERS structures, it is very difficult to achieve broadband plasmon wavelengths when using only a single antenna structure. Thus, antennas with different sizes, gap spacings, or dielectric spacers would have to be applied according to the excitation laser

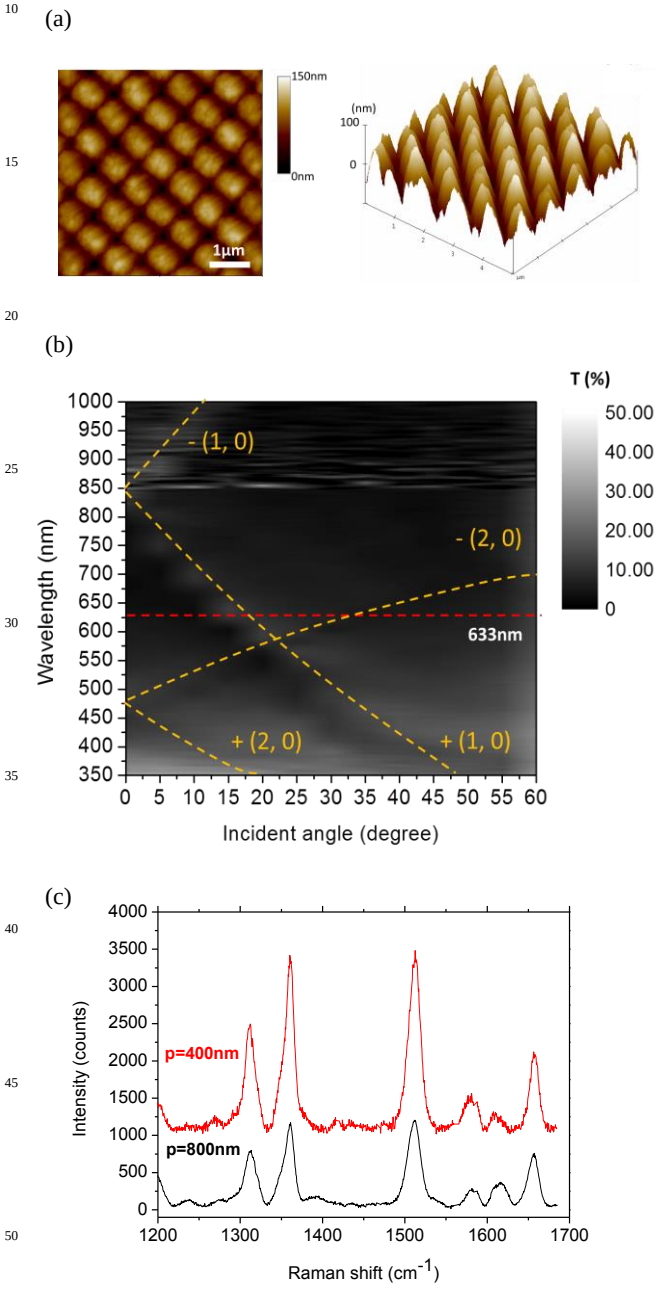

Fig. 7 (a) Top-view and 3D AFM images and (b) SPR dispersion diagram of an imprinted Ag mirror having a period of 800 nm. (c) SERS spectra of 10^{-6} M R6G adsorbed on NP-imprinted mirrors having periods of 400 and 800 nm, respectively.

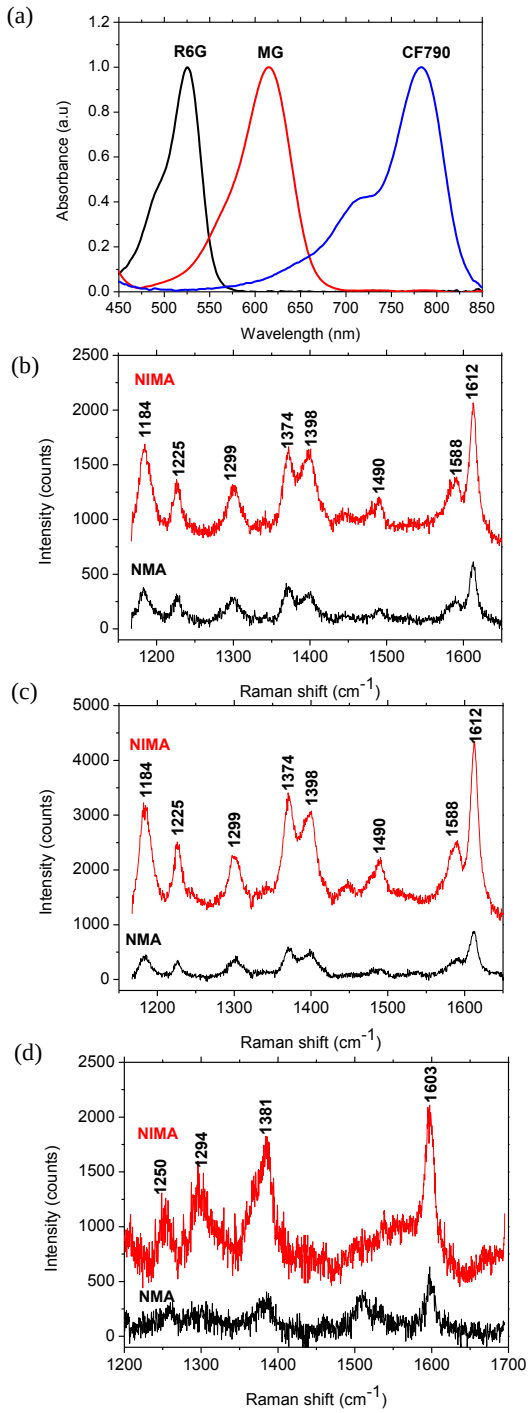

Fig. 8 (a) Absorbance spectra of R6G, MG, and CF790. (b, c) SERRS spectra of 10^{-6} M MG adsorbed on the NMA and NIMA under excitation at 633 nm with angles of incidence of (b) 0 and (c) 35°. (d) SERRS

spectra of 10^{-6} M CF790 adsorbed on the NMA and NIMA under excitation at 785 nm with an angle of incidence of 25°.

wavelength and the absorbance regime of the various analytes. As described above, the NIMA would be a versatile substrate for SERRS applications because of wide-ranged coupling between the LSPR of the NPs and the periodic structure–excited SPR of the imprinted mirror.

We used the NMA and NIMA to detect three analytes

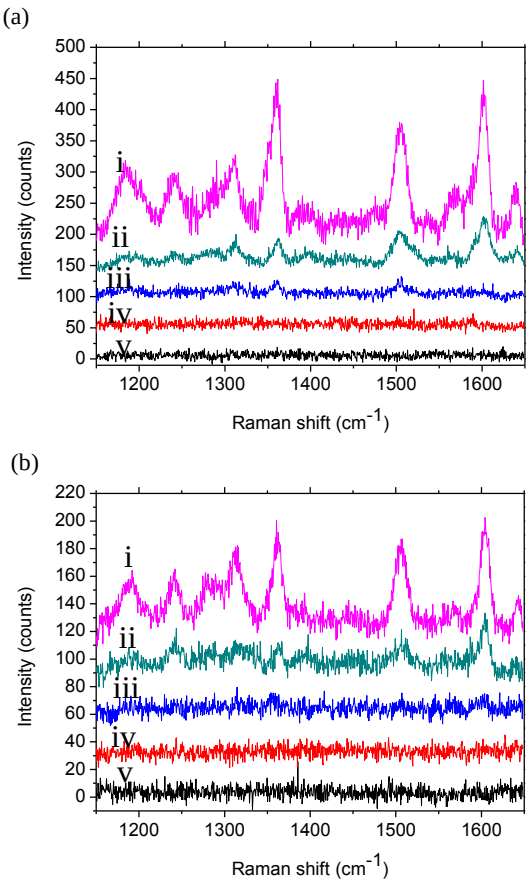

Fig. 9 SERS spectra of (a) 10^{-12} M and (b) 10^{-15} M R6G adsorbed on the NIMA, the NMA, NPs-on-glass substrates, an imprinted mirror, and a flat mirror (i: NIMA; ii: NMA; iii: NPs on glass; iv: imprinted mirror; v: flat mirror).

possessing distinct absorbance regimes (Fig. 8a)—R6G (λ_{abs} = 525 nm), malachite green (MG; λ_{abs} = 615 nm), and CF790 dye (λ_{abs} = 783 nm). Due to the distinct absorbance regime of the analytes, we used different excitation wavelengths to measure their SERRS signals. Here, we applied three different excitation wavelengths—532, 633, and 785 nm—that were close to the absorption wavelengths of the analytes, allowing the resonance Raman signals to be obtained. Fig. 4 displays the SERS spectra of R6G recorded at various excitation wavelengths and angles of incidence. The SERS spectra recorded under excitation at 532 nm exhibited most of the characteristic Raman lines of R6G—at 1273, 1311, 1360, 1507, 1573, 1607, and 1647 cm^{-1}. We assign the signal at 1273 cm^{-1} to the C–O–C stretching mode and the other lines to aromatic C–C stretching modes.[44] Unlike the SERS spectra obtained with excitation of the NMA structure at other wavelengths, excitation at 532 nm provided additional resonance enhancement, leading to the most characteristic Raman spectrum of R6G. For example, Fig. 4d and 4e display the SERS spectra of R6G adsorbed on the NMA upon excitation at 633 nm (the signal at 1273 cm^{-1} is almost absent) and 785 nm (additional signals became very weak), respectively. On the other hand, because the absorbance regime of MG was located near 633 nm, the SERS substrate having its plasmon wavelength at 633 nm was the most suitable for detecting this analyte; conveniently, we could enhance the electric field intensity of the NIMA at 633 nm by simply changing the angle of incidence to 35°. Fig. 8b and 8c display the SERRS spectra of MG adsorbed on the NMA and the NIMA with excitation at 633 nm at angles of incidence of 0 and 35°, respectively. Because of strong electromagnetic coupling, the NIMA enhanced the Raman signals of MG to a greater extent than did the NMA. Compared with the SERS spectra obtained with excitation at other wavelengths, the SERRS spectra excited at 633 nm featured the most characteristic Raman lines of MG (1184, 1225, 1299, 1374, 1398, 1490, 1588, and 1612 cm^{-1}), due to the additional resonance enhancement. On the other hand, many characteristic lines were almost absent in the SERS spectra of MG adsorbed on the NMA structure under excitation at 532 or 785 nm (Fig. S3). Although the NMA experienced electromagnetic enhancement at 532 nm, it could not induce all of the Raman signals. In comparison, the stronger electromagnetic enhancement of the NIMA induced all of the Raman signals at the resonance excitation wavelength—and most of them even at non-resonance wavelengths (Fig. S3). Therefore, the SERS and SERRS performances of the NIMA were superior to those of the NMA. Similarly, we readily obtained the NIR-SERRS spectra of the dye CF790 when using the NIMA with excitation at 785 nm (Fig. 8d and S4). Notably, we attribute the stronger Raman scattering intensity to the resonance enhancement.

In this study we did not, however, compare the intensities of the signals in the SERS spectra under different excitation wavelengths or angles of incidence, for the following reasons. First, the Raman scattering cross-section of the analytes was inversely proportional to the excitation wavelength to the power of four. Second, the laser light sources (as described in the Methods) that we used in these experiments had different input powers, which would also influence the SERS intensity. Third, the intensity of the electric field normal to the NMA or NIMA surface would increase upon increasing the angle of incidence, resulting in different coupling strengths. For these reasons, any comparisons of the intensities after excitation at different wavelengths or angles of incidence would give no additional information about the resonance enhancement. Nevertheless, we could still observe resonance enhancement for the most-characteristic Raman lines when excited by the resonance wavelengths. Therefore, the NIMA possessed a wide working spectral regime, from the visible to the NIR; such a broadband operating range in a single structure is very difficult to achieve when using an NMA or another type of SERS substrate, as mentioned above.

Finally, we compared the SERS performance of the NIMA with those of other SERS-active substrates. Here, we prepared a

NIMA, an NMA, three NPs-on-glass substrates (with the same number density of NPs on each surface), and an imprinted mirror and a flat mirror (both without NPs). The corresponding angle-dependent transmission or reflection spectra of these substrates were provided in the supplementary information, and the plasmonic properties of these substrates could be readily observed (Fig. S1 and S5). We measured the SERS spectra of 1 pM (10^{-12} M) and 1 fM (10^{-15} M) R6G adsorbed on these SERS-active substrates at an angle of incidence of 35° under excitation at 633 nm—far from the LSPR wavelength of an isolated Ag NP. The SERS spectra in Fig. 9a and 9b reveal that the NIMA enhanced the Raman signals dramatically when compared with other substrates. Because of weaker coupling between the NPs and the underlying flat mirror at a wavelength of 633 nm, the Raman signals of the NMA were much less intense than those of the NIMA. In addition, the Ag NPs on glass contributed little SERS enhancement to the Raman signals. Because of the mismatch between the LSPR wavelength of the Ag NPs (ca. 430 nm) and the excitation wavelength (633 nm), the Ag NPs on glass were less-efficient SERS-active substrates when compared with the NIMA. Finally, the SERS performance of the imprinted mirror lacking Ag NPs was better than that of the flat mirror, but worse than that of the NIMA, the NMA, or the NPs on glass. Therefore, we can confirm that coupling between the LSPR and the periodic structure–excited SPR was responsible for the largest electromagnetic enhancement, and that our NIMAs are more robust, broadband, SERS-active substrates than are other common SERS-active substrates. In addition, their limits of detection could reach less than 10^{-15} M.

Conclusions

In summary, we have used a direct nanoimprint-in-metal method to prepare incident angle–tunable, broadband, ultrahigh-sensitivity NIMAs. Without the need for developing or etching processes, we obtained 2D periodic structures on mirror surfaces. The strong electric field intensity of the NIMA arose from electromagnetic coupling between the LSPR of the NPs and the periodic structure–excited SPR on the imprinted mirror. Notably, the electric field intensity in the NIMA was enhanced to a greater degree than those in the conventional NMA or other NP-based SERS-active substrates. Moreover, the period of the textured structure of the NIMA and the angle of incidence could be varied to modulate the SPR wavelength. Our NIMAs are broadband SERS-active substrates possessing working regime from the visible to the NIR. Compared with other SERS-active substrates, the NIMAs achieved their broadband enhancement from single structures, rather than the application of various substrates having different periods or morphologies. In addition, the SERS performance of a NIMA increased when it featured a deeper, more consistent structure. On the other hand, the SPR modes also influenced the SERS performance. A lower-order SPR mode provided stronger intensities; therefore, the greatest electric field intensity occurred after coupling the LSPR with the lower SPR mode. In conventional NP-based SERS-active substrates and the NMA, it can be difficult to achieve a wide working regime using a single type of structure; therefore, the NIMAs are more suitable for SERRS applications. By changing the angles of incidence, we could obtain the SERRS spectra of analytes (e.g., R6G, MG, CF790) that absorb over ranges from the visible to the NIR. We have also demonstrated that the NIMA is superior to other common SERS-active substrates, with the detection of R6G possible at a concentration as low as 10^{-15} M.

Methods

Imprinted Ag Mirrors: Fabrication and Characterization

A 50-nm-thick Ag film was first deposited on a 365-μm-thick PC substrate by operating a sputtering system at a rate of 3 Å/s. The Si master mold was fabricated using electron beam lithography. The nanoimprint-in-metal method was performed by imprinting the Si master mold onto the Ag film at various pressures. The system was maintained at 150 °C during the imprinting process. After imprinting, the Ag film/Si master mold was cooled to room temperature and then demolded. The morphologies and depths of the imprinted mirrors were measured using a scanning electron microscopy (JEOL, JSM-6700F) atomic force microscopy (Veeco, D5000); Angle-dependent zero-oprder transmission and reflection spectra were measured using an optical spectrophotometer (Hitachi, U4100) with TM-polarized incident light. Angle-dependent zero-order transmission spectra of imprinted mirrors was measured in order to obtain the SPR dispersion diagram.

NP-imprinted mirror antennas (NIMAs)

The NIMA was fabricated by self-assembling Ag NPs (diameter: 100 nm) onto the imprinted mirror. First, the imprinted Ag mirror was immersed in 1 mM (3-aminopropyl)trimethoxysilane (APTMS, Sigma–Aldrich) in EtOH and incubated for 12 h. After a self-assembled monolayer (SAM) of APTMS had formed on the imprinted Ag mirror surface, the imprinted mirror was rinsed sequentially with EtOH and deionized water to remove any non-bound APTMS. An aliquot (400 μL) of a Ag NP suspension (Ted Pella) was placed on the imprinted Ag mirror for 1 h. After the Ag NPs had immobilized on the imprinted mirror surface, the samples were rinsed with deionized water and dried under a flow of N_2. The SAM of APTMS acted as a spacer that helped to bind the Ag NPs while separating them from the underlying mirror. The NMAs and the NPs-on-glass substrates were also fabricated using this self-assembly process.

Surface-enhanced Raman scattering (SERS) measurement

The NMAs and NIMAs were incubated in analyte solutions of R6G (Sigma–Aldrich), MG (Sigma–Aldrich), and the laser dye CF790 (Sigma–Aldrich) for 12 h, all at a concentration of 10^{-6}M. All materials were used as received. For measurements at ultralow concentrations, the NIMA, the NMA, the NPs-on-glass substrates, the imprinted mirror, and the flat mirror were incubated in 1 pM (10^{-12} M) and 1 fM (10^{-15} M) R6G solutions for 12 h to determine the limits of detection. Raman spectra were recorded using a commercial Raman microscope (Protrustech, BWII) equipped with a monochromator having a focal length of 75 cm. The excitation laser lines were 532 nm (diode laser), 633 nm (He-Ne laser), and 785 nm (diode laser). The incident powers on the samples were 2 mW (532 nm), 1.7 mW (633 nm), and 7.3 mW (785 nm) when the analytes were R6G and MG; because of its high fluorescence, the incident powers on the samples were

attenuated to 0.52 mW (532 nm), 0.17 mW (633 nm), and 0.73 mW (785 nm) when measuring the SERS spectra of CF790. In all measurements, the incident light was TM-polarized, a 100× objective lens was used, and the signal integration time was 1 s under excitation at 532 nm and 10 s under excitation at 633 or 785 nm. The samples were positioned on a rotation stage so that the angles of incidence could be tuned throughout the SERS measurement process.

Acknowledgements

We thank the Ministry of Science and Technology, Taiwan, for supporting this study under contracts MOST-103-2221-E-002-041-MY3 and MOST-103-2221-E-002-092-MY3

Notes and references

[a] *Department of Materials Science and Engineering, National Taiwan University, No. 1, Sec. 4, Roosevelt Road, Taipei, 10617 Taiwan (R.O.C) Fax: +886 2 2364 4562; Tel: +886 2 3366 3240; E-mail: hsuenlichen@ntu.edu.tw*

† Electronic Supplementary Information (ESI) available: Additional SERS spectra of malachite green and CF790 dye. See DOI: 10.1039/b000000x/

1 S. Mubeen, S. Zhang, N. Kim, S. Lee, S. Krämer, H. Xu, M. Moskovits, *Nano Lett.* 2012, **12**, 2088–2094.
2 S. Y. Chen, J. J. Mock, R. T. Hill, A. Chilkoti, D. R. Smith, A. A. Lazarides, *ACS Nano*, 2010, **4**, 6535-6546.
3 J. Jung, K. Na, J. Lee, K. W. Kim, J. Hyun, *Anal. Chim. Acta* 2009, **651**, 91–97.
4 L. He, M. D. Musick, S. R. Nicewarner, F. G. Salinas, S. J. Benkovic, M. J. Natan, C. D. Keating, *J. Am. Chem. Soc.* 2000, **122**, 9071–9077.
5 R. T. Hill, J. J. Mock, A. Hucknall, S. D. Wolter, N. M. Jokerst, D. R. Smith, A. Chilkoti, *ACS Nano*, 2012, **6**, 9237–9246.
6 M. W. Knight, Y. Wu, J. B. Lassiter, P. Nordlander, N. J. Halas, *Nano Lett.* 2009, **9**, 2188-2192.
7 D. Y. Lei, A. I. Ferna´ndez-Domı´nguez, Y. Sonnefraud, K. Appavoo, R. F. Haglund, Jr., J. B. Pendry, S. A. Maier, *ACS Nano*, 2012, **6**, 1380-1386.
8 H. Gehan, L. Fillaud, M. M. Chehimi, J. Aubard, A. Hohenau, N. Felidj, C. Mangeney, *ACS Nano*, 2010, **4**, 6491-6500.
9 C. Lumdee, S. Toroghi, P. G. Kik, *ACS Nano*, 2012, **6**, 6301–6307.
10 F. Le, N. Z. Lwin, J. M. Steele, M. Kall, N. J. Halas, P. Nordlander, *Nano Lett.*, 2005, **5**, 2009-2013.
11 G. Ctistis, P. Patoka, X. Wang, K. Kempa, M. Giersig, *Nano Lett.*, 2007, **7**, 2926-2930.
12 T. W. Ebbesen, H. J. Lezec, H. F. Ghaemi, T. Thio, P. A. Wolff, *Nature*, 1998, **391**,667–669.
13 H. Gao, J. Henzie, T. W. Odom, *Nano Lett.* 2006, **6**, 2104-2108.
14 K. G. Lee, Q. H. Park, *Phys. Rev. Lett.* 2005, **95**, 103902-1-103903-4.
15 S. Y. Chuang, H. L. Chen, S. S. Kuo, Y. H. Lai, C. C. Lee, *Opt. Express*, 2008, **16**, 2415-2422.
16 C. C. Yu, K. H. Ho, H. L. Chen, S. Y. Chuang, S. C. Tseng, W. F. Su, *Biosens. Bioelectron.*, 2012, **33**, 267– 273.
17 M. D. He, Z. Q. Gong, S. Li, Y. F. Luo, J. Q. Liu, X. Chen, W. Lu, *J. Appl. Phys.* 2010, **108**, 093520-1-093520-6.
18 L. Wang, B. Xu, W. Bai, J. Zhang, L. Cai, H. Hu, G. Song, *Plasmonics*, 2012, **7**, 659–663.
19 Y. C. Chen, Y. T. Chang, H. H. Chen, F. T. Chuang, C. H. Cheng, S. C. Lee, *IEEE Photonic. Technol. Lett.*, 2013, **25**, 47-50.
20 M. J. Kofke, D. H. Waldeck, G. C. Walker, *Opt. Express*, 2010, **18**, 7705-7713.
21 A. Campion, P. Kambhampati, *Chem. Soc. Rev.*, 1998, **27**, 241-250.
22 P. Hildebrandt, M. Stockburger, *J. Phys. Chem.* 1984, **88**, 5935-5944.
23 S. Habuchi, M. Cotlet, R. Gronheid, G. Dirix, J. Michiels, J. Vanderleyden, F. C. De Schryver, J. Hofkens, *J. Am. Chem. Soc.*, 2003, **125**, 8446-8447.
24 G. F. S. Andrade, J. G. Hayashi, M. M. Rahman, W. J. Salcedo, C. M. B. Cordeiro, A. G. Brolo, *Plamonics*, 2013, **8**, 1113–1121.
25 N. G. Greeneltch, A. S. Davis, N. A. Valley, F. Casadio, G. C. Schatz, R. P. Van Duyne, N. C. Shah, *J. Phys. Chem. A* 2012, **116**, 11863−11869.
26 S. K. Jha, Z. Ahmed, M. Agio, Y. Ekinci, J. F. Löffler, *J. Am. Chem. Soc.* 2012, **134**, 1966−1969.
27 D. O. Sigle, E. Perkins, J. J. Baumberg, S. Mahajan, *J. Phys. Chem. Lett.* 2013, **4**, 1449−1452.
28 A. J. Pasquale, B. M. Reinhard, L. Dal Negro, *ACS Nano*, 2011, **5**, 6578–6585.
29 A. J. Pasquale, B. M. Reinhard, L. Dal Negro, *ACS Nano*, 2012, **6**, 4341–4348.
30 H. Aouani, H. Sˇ ı´pova´ , M. Rahmani, M. Navarro-Cia, K. Hegnerova´, J. Homola, M. Hong, S. A. Maier, *ACS Nano*, 2013, **7**, 669-675.
31 M. Navarro-Cia, S. A. Maier, *ACS Nano*, 2012, **6**, 3537–3544.
32 H. Aouani, M. Navarro-Cia, M. Rahmani, T. P. H. Sidiropoulos, M. Hong, R. F. Oulton, S. A. Maier, *Nano Lett.*, 2012, **12**, 4997−5002.
33 S. V. Boriskina, L. Dal Negro, *Opt. Lett.* 2010, **35**, 538-540.
34 S. Y. Chou, P. R. Krauss, P. J. Renstrom, *J. Vac. Sci. Technol. B* 1996, **14**, 4129-4133.
35 L. J. Guo, *Adv. Mater.* 2007, **19**, 495–513.
36 S. Y. Chou, P. R. Krauss, P. J. Renstrom, *Science*, 1996, **272**, 85-87.
37 W. D. Li, F. Ding, J. Hu, S. Y. Chou, *Opt. Express*, 2011, **19**, 3925-3936.
38 R. Alvarez-Puebla, B. Cui, J. P. Bravo-Vasquez, T. Veres, H. Fenniri, *J. Phys. Chem. C* 2007, **111**, 6720-6723.
39 T. W. Ebbesen, H. J. Lezec, H. F. Ghaemi, T. Thio, P. A. Wolff, *Nature*, 1998, *391*, 667-669.
40 Y. Zhu, H. Kuang, L. Xu, W. Ma, C. Peng, Y. Hua, L. Wang, C. Xu, *J. Mater. Chem.*, 2012, **22**, 2387-2391.
41 W. Ma, M. Sun, L. Xu, L. Wang, H. Kuang, C. A. Xu, *Chem. Commun.*, 2013, **49**, 4989-4991.
42 G. H. Jeong, Y. W. Lee, M. Kim, S. W. Han, *J. Colloid Interface Sci.* 2009, **329**, 97–102.
43 A. M. Schwartzberg, T. Y. Oshiro, J. Z. Zhang, T. Huser, C. E. Talley, *Anal. Chem.* 2006, **78**, 4732-4736.
44 P. Hildebrandt, M. Stockburge, *J. Phys. Chem.* 1984, **88**, 5935-5944.